Direct identification and determination of conformational response in adsorbed individual non-planar molecular species using non-contact atomic force microscopy

Florian Albrecht[1], Felix Bischoff[2], Willi Auwärter[2], Johannes V. Barth[2], and Jascha Repp[1]

1 Institute of Experimental and Applied Physics, University of Regensburg, 93053 Regensburg, Germany
2 Physik-Department E20, Technische Universität München, James-Franck-Straße 1, 85748 Garching, Germany

Abstract

In recent years atomic force microscopy (AFM) at highest resolution was widely applied to mostly planar molecules, while its application towards exploring species with structural flexibility and a distinct 3D-character remains a challenge. Herein, the scope of non-contact AFM is widened by investigating subtle conformational differences occurring in the well-studied reference systems 2H-TPP and Cu-TPP on Cu(111). Different saddle-shape conformations of both species can be recognized in conventional constant-height AFM images. To unambiguously identify the behavior of specific molecular moieties we extend data acquisition to distances that are inaccessible with constant-height measurements by introducing vertical imaging – that is, AFM mapping in a plane perpendicular to the sample surface. Making use of this novel technique the vertical displacement of the central Cu atom upon tip-induced conformational switching of Cu-TPP is quantified. Further, for 2H-TPP two drastically different geometries are observed, which are systematically characterized. Our results underscore the importance of structural flexibility in adsorbed molecules with large conformational variability and, consequently, the objective to characterize their geometry at the single-molecule level in real space.

Key words: *nc-AFM, single molecules, 3D structure, CO tip, 2H-TPP, Cu-TPP*

Porphyrins and the closely related phthalocyanines provide a potpourri of functionalities as evidenced by their potential in catalysis[1], molecular electronics[2] or spintronics[3], to name a few examples. Hence they serve as extremely versatile building blocks for 2D-architectures[4-6]. In addition, their properties can be tuned by modifications within their macrocycle[2,7], by chemical engineering of the molecular periphery[8] or by suitable choice of the underlying support[9-11]. Porphyrins with meso-

substituents such as tetraphenylporphyrin (TPP) typically exhibit a saddle-shape conformation of their macrocycle upon adsorption onto coinage metal surfaces.[7,11-17] This saddle-shape adaptation leads to distinct molecular properties such as unusual ligation schemes of adducts[18] or molecular self-assembly[7]. Hence, a prerequisite for the development of a (technological) application is the understanding and control of properties of individual molecules at the molecular and even the atomic scale. This implies that conformational characterisations are essential. The experimental techniques for molecular nanoscience at interfaces employed so far are mainly scanning tunnelling microscopy (STM), scanning tunnelling spectroscopy (STS), X-ray photoelectron spectroscopy (XPS) and near-edge-X-ray absorption fine structure (NEXAFS).[4,6,19] While XPS can yield averaged information about the chemical state of the macrocycle for example, with STM, topographic and structural investigations of porphyrin arrays as well as single molecules can be carried out in real space. The high lateral resolution of low-temperature STM allows gathering local information at the single-molecule level. The convolution of topography and electronic structure in STM data, however, generally prohibits a direct interpretation in terms of the sample's geometric shape. Information on molecular conformation could so far only be obtained by synchrotron-based NEXAFS measurements[17], with the drawback of averaging over countless molecules and – most importantly – all molecular moieties, or for specific cases by comparison of STM data with calculated images.[12,20,21]
Over the last years, small-amplitude non-contact atomic force microscopy (AFM) in the form of frequency-modulation AFM (FM-AFM) with CO or other functionalized tips has been established as an extremely powerful and versatile tool for structure analysis of surface-confined organic molecules in real space[22-34]. Its capability to resolve individual molecular bonds allows a direct identification of molecular structures[22-26], conformation[27] and even changes thereof upon chemical reactions.[24,28-31] So far, FM-AFM investigations have mainly addressed flat species adsorbing (nearly) coplanar to the surface, and merely a few non-planar molecules were investigated in constant height[27,32,33,35,36]. Additionally, $\Delta f(z)$-mapping has been applied to gain quantitative insights on molecular features that could already be qualitatively accessed with standard techniques.[33,36] Very recently, a time-consuming three-dimensional $\Delta f(z)$-data set was analysed to identify the helical structure of a molecule[24] and a two-pass imaging mode was used to depict a three dimensional molecular structure[34].

In this low-temperature FM-AFM study we analyze subtle differences in the conformation of individual non-planar free-base and copper-metalated tetraphenylporphyrin molecules (2H-TPP and Cu-TPP) adsorbed on Cu(111) employing FM-AFM with CO-functionalized tips. Constant-height imaging allows a qualitative characterization of the substrate-induced saddle-shape conformation apparent in the orientation of different molecular subunits[32,35], but fails for molecular identification

of conformationally similar species, for determining small conformational changes and for quantitative assessments. Vertical imaging is introduced as a useful tool enabling data acquisition at much closer tip-sample spacing than in conventional constant-height imaging and therefore yields information elusive to other methods. The aforementioned FM-AFM techniques try to circumvent imaging restrictions arising from molecular non-planarity by adapting the imaging plane parallel to the molecular structure. By contrast, our novel approach deliberately generates surface-perpendicular images and only therefore allows for the direct identification of minute conformational differences within individual molecules. In comparison to a full three-dimensional dataset it largely reduces data acquisition time by reduction of data recording to one single plane. It turns out that 2H-TPP exhibits a flatter macrocycle than Cu-TPP under low temperature preparation conditions and that Cu-TPP can adopt two states by tip-induced switching. Finally, the macrocycle of 2H-TPP is transformed from a moderate saddle-shape into a strongly deformed configuration, which turns out to be the configuration of 2H-TPP when deposited onto a substrate held at room temperature. Our new approach thus provides quantitative structural information valuable for, e.g., benchmarking theoretical models in density functional theory (DFT). The observed large structural variability of the molecular geometries underscores the importance of characterizing them at the single-molecule level, going beyond space-averaging techniques.

Before discussing the experimental results, we will briefly introduce the geometry of 2H-TPP and Cu-TPP on Cu(111) (Fig. 1a). These two exemplary tetrapyrrole species are well understood in surface science and their molecular structure has been investigated with a multitude of experimental approaches.[4,6] In a simplified view, the conformation of TPP on a surface is determined by the balance of surface interactions and steric interference of different molecular moieties. The rotation of the phenyl legs is linked to the tilting of the pyrrole units of the macrocycle[37]. Flatter phenyl legs, i.e., small dihedral angles between the legs and the surface plane, cause a stronger deformation of the macrocycle. Vice versa, a planar macrocycle will lead to more upright legs. Upon adsorption onto metal substrates, many porphyrin derivatives adapt a saddle-shape conformation.[7,11-17] The saddle-shape describes a tilting of the pyrrole moieties out of the macrocyclic plane. On Cu(111), the two iminic nitrogens point towards the surface while the pyrrolic/aminic nitrogens point away from it (compare Fig. 1a). For 2H-TPP on Cu(111) space-averaging NEXAFS measurements of a monolayer coverage indicate out-of-plane rotation angles of ≈ 50° and 20° for the macrocycle moieties and the phenyl legs, respectively. Upon self-metalation the macrocycle of Cu-TPP flattens and the tilt angles of macrocycle and phenyl legs roughly interchange.[17,38] Accordingly, TPP molecules do not comprise any hydrocarbon ring systems parallel or nearly parallel to the surface in contrast to most molecular systems assessed so far in FM-AFM studies. For molecules with a pronounced 3D conformation with

many internal degrees of freedom − as in the case of TPPs − a detailed structural characterization is not possible from constant-height FM-AFM images[34]. Nevertheless, constant-height imaging can yield useful information about the molecular conformation. Molecular moieties protruding higher above the surface interact repulsively with the tip at larger distances.[24,33,39] Therefore, conclusions about relative height differences within a single molecule and for neighboring molecules can be drawn from constant-height FM-AFM imaging.

Figure 1 shows constant-current STM and constant-height AFM data of a low-temperature preparation with Cu-TPP (left) and side-by-side a 2H-TPP (right) in the same adsorption orientation for direct comparison. For information on how the molecules were identified in the first place, please see further below. In contrast to previous reports applying different preparation protocols[15], here Cu-TPP and 2H-TPP show only very subtle differences in STM images (Fig. 1b). In line with the alike STM appearance, the two species only exhibit faint differences in contrast evolution of constant-height frequency shift (Δ*f*) imaging for decreasing tip-sample spacing (Fig. 1c–e).

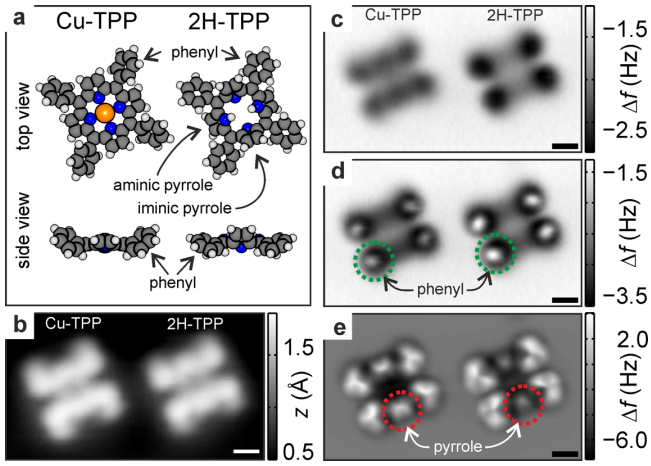

Figure 1. Conformations of copper tetraphenylporphyrin (Cu-TPP) and free-base tetraphenylporphyrin (2H-TPP) on Cu(111). (a) Top and side view of a model of Cu-TPP and 2H-TPP. Conformations of adsorbed species are taken from [17]. While 2H-TPP exhibits a pronounced saddle-shape, Cu-TPP is only slightly saddle-shaped with an almost flat macrocycle. (b) Constant-current STM image (setpoint (SP): I = 2 pA, U = 100 mV) of Cu-TPP (left) and 2H-TPP (right) in the same adsorption orientation on Cu(111) following low-temperature deposition. (c–e) Constant-height FM-AFM images approaching the surface from SP +1 Å to SP +0.4 Å to SP -0.8 Å. STM SP: I = 2 pA, U = 100 mV. Scale bars are 5 Å. The contrast evolution indicates that – in agreement with previous work – flatter phenyl legs (highlighted by green markers in (d)) are accompanied with a stronger deformation of the macrocycle that can be seen in the tilt of the pyrrole rings (see red markers in

(e)). The observed flatness of Cu-TPP in comparison to 2H-TPP contradicts the molecular models reported in the literature as depicted in (a).

Mapping Δ*f* at constant height results in the evolution of the contrast from dark areas above the molecule (attractive background) for large tip heights to sub-molecular resolution of the molecular structure at close distances, owing to laterally confined repulsive interactions at the molecular bonds that result in a bright contrast.[40] Molecules with pronounced 3D character have been shown to exhibit bright Δ*f* contrast at highest molecular parts first. [24,33,39] In the Δ*f* image recorded with the largest tip-sample spacing, the dark attractive background indicates the outline of each molecule (Fig. 1c). Then, the phenyls interact repulsively (see green markers in Fig. 1d) and at closer distances two opposing pyrroles at the macrocycle follow (red rings in Fig. 1e). None of the ring systems comprised in the molecular species can be directly imaged with single bond resolution due to four possible constraints: i) the tilt is too large[24,27], ii) other moieties might interfere, as for example the pyrroles lie above/below the phenyls (see model in Fig. 1a), iii) the necessary tip approach cannot be achieved due to other considerably higher moieties that would cause a tip crash and iv) the flexible CO-tip can be influenced laterally by neighboring molecular parts[22]. Although the strong 3D character of the molecules prohibits direct imaging of the entire molecular structure, the evolution of repulsively interacting molecular parts fits very well the saddle-shape conformation and correctly reproduces the dependence of the phenyl rotation and the tilt of pyrrole units qualitatively. The molecule, the phenyl legs of which appear bright at a greater distance (Fig. 1d), has to be approached closer in order to detect the pyrroles (Fig. 1e). Equivalently, in the picture of the saddle shape, more upright phenyls correspond to a flatter macrocycle. This means that the macrocycle of 2H-TPP seems to be more flat than for Cu-TPP, which is not in line with previous NEXAFS results[17]. As will be discussed below, this discrepancy is caused by the different sample temperature upon deposition of molecules of this and the former study[17]. The differences in the relative heights of distinct molecular moieties as described above allow distinguishing the two species straightforwardly. However, due to the subtle differences between Cu-TPP and 2H-TPP in conventional constant-height imaging, a comparison of individual molecules from different preparations, with different tips or even experimental setups is not reliable. Instead, this can only be done when directly comparing the two species side-by-side (i.e., same imaged area with same tip and same setpoint). In contrast, as will be shown in the following, vertical imaging allows one to unambiguously identify the molecules.

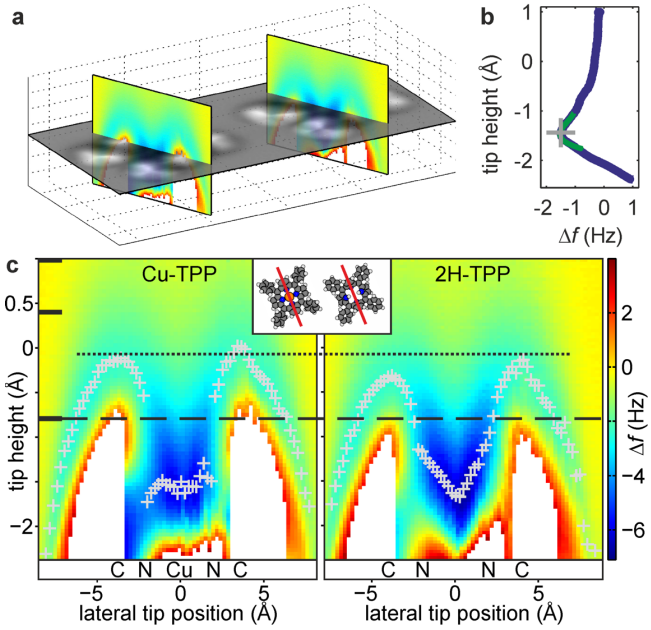

Figure 2. Acquisition and analysis of vertical images. (a) 3D representation of vertical images recorded in a mirror plane of each molecule. (b) Δ*f*(*z*) frequency shift-distance curves were recorded for each lateral tip position along the mirror plane. The grey crosses in (b,c) mark the minimum of each background subtracted Δ*f*(*z*) curve. (c) Δ*f*(*z*) curves are color coded and displayed as tip height *z* vs. lateral position to generate vertical images. In white areas, a safety Δ*f* limit is exceeded and the measurement is aborted, such that there are no data points available[41]. Positions of the atoms along the mirror plane are indicated beneath the maps. The inset in (c) shows the mirror planes in which the images were recorded. The contour of the Δ*f*(*z*) minima above the center of the Cu-TPP macrocycle is almost flat, while for 2H-TPP a V-shape can be identified. The thin dotted line serves as guide to the eye for relative height comparison of the highest molecular parts. Both images were recorded with the same tip from the same SP. The large ticks in (c) indicate the tip height at which the constant-height images depicted in Fig. 1c–e were recorded. Note that the closest constant-height image was recorded at the limit of safely accessible tip heights (see dashed line). Zero at the tip height scale corresponds to the STM SP height of 2 pA and 100 mV on copper. The vertical imaging technique allows recording the Δ*f* signal at the center of the molecule at close distances, which are not accessible to constant-height AFM imaging. Importantly, it is exactly this region, where the decisive features in the Δ*f* signal to discriminate the molecules occur.

To acquire vertical images, sets of frequency shift versus distance curves are recorded following a method introduced by Mohn et al.[41] These provide Δ*f* images in planes perpendicular to the sample surface. The imaging planes were set to coincide with one of the vertical molecular mirror planes according to the molecular C_{2v} symmetry as indicated by the red lines in the inset in Fig. 2c. Note that

the chosen acquisition planes run across the macrocycle only and disregard the meso-substituents. Images were also acquired in the other of the two mirror planes and yield similar contrast at the center of the macrocycle (for further details see SI Fig. S1). For each frequency shift-distance curve, the minimum in $\Delta f(z)$ is determined after background subtraction and its vertical position z_{min} is highlighted by a grey cross in the 2D plots in Fig. 2c. Both molecules show two peaks along the profiles of minimum positions that can be assigned to the two opposing iminic pyrroles of the macrocycle. The profiles nicely reproduce the constant-height data, confirming that Cu-TPP exhibits higher pyrrole moieties (see thin dotted line in Fig. 2c). Importantly, the appearance of the minima in vertical images reveals differences between the molecules at the respective macrocycle regions, i.e. in between the pyrrole peaks. For Cu-TPP it is flat while for 2H-TPP a pronounced V-shape can be identified (compare Fig. 2c). To be able to assign these distinct features to a molecular species, reference data was acquired for monomolecular sample preparations first. These results were reproducible for several different tips, all adsorption orientations and four different sample preparations and therefore represent general fingerprints of each molecular species. With the help of these fingerprints in the vertical images, unambiguous molecular identification becomes feasible. Based on the experimental evidence we thus conclusively assign the left molecule in Fig. 1 to a Cu-TPP and the right one to 2H-TPP. The decisive features to discriminate the molecules are located ≈ 1 Å closer to the sample than the constant-height image at closest tip-sample spacing (see dashed line in Fig. 2c). Recording conventional constant-height images at a reduced tip height is not possible, as there the large tip molecule interactions would result in undesired lateral displacement or pick up of the molecule. Moreover, data acquisition for a vertical image is much faster and simpler than recording an entire 3D data set[24,42]. Unfortunately, determining the adsorption angle of single substituents via $\Delta f(z)$ measurements analogous to an entire molecule[36] was unsuccessful due to the interference of other molecular parts resulting in CO deflections at the tip.

Individual Cu-TPP molecules can be reversibly switched between two conformational states, adding a new observation to porphyrin switches.[43,44] These two states exhibit a clearly discernible current distribution across the molecule (Fig. 3a,c) and Δf signal (Fig. 3b,d) in conventional constant-height data as well as obviously different vertical images (Fig. 3e,f). We henceforth refer to these as state 1 and 2, whereby the former is the as-deposited species following exposure of the sample at low temperature. It is reasonable to assume, that a smaller difference Δh in z_{min} values between the pyrroles and the central metal ion corresponds to a flatter macrocycle (see Fig. 3e,f). Hence state 2 appears to be more flat (Δh_{s1} = 1.5 Å > Δh_{s2} = 1.2 Å). This is especially articulated in the vertical images in the second mirror plane (SI Fig. S2). The vertical image along the second axis also allows the distinction between 2H-TPP and the switched Cu-TPP molecule (compare Fig. S1d and Fig. S2b).

Due to steric hindrance, a flattened macrocycle results in more upright legs and therefore elevates the central metal ion by Δh_{Cu} = 0.5 Å (compare thin dotted lines in Fig. 3e,f). Interestingly, the current channel shows more contribution above two pyrroles for state 2 compared to state 1 and would therefore at first glance – when interpreted as being directly related to geometry - wrongly suggest a stronger macrocycle deformation. Intriguingly, the vertical displacement of the central copper atom does not affect the tunneling current at the center of the molecule. This underlines the difficulty of assigning conformations from STM data alone, which may yield misleading vertical information[25].

The origin of the discrepancy between the previously reported conformations and the findings described above lies in the different sample preparation conditions. On the one hand, in the previous reports TPP was sublimed onto a substrate held at room temperature, while here molecules were evaporated onto a sample held below 10 K. Apparently molecules have to overcome an energy barrier for adapting their energetically most favorable conformation upon adsorption onto a cold surface but seem to be trapped in a metastable conformational state. Additionally, an increased molecular coverage deposited at room temperature often entails island formation. Thus intermolecular interactions become operative that might affect the conformation of individual molecules through, e.g., T-type interaction[15,45-48], and thereby Cu-TPP might switch into the state 2 as described. Apart from preventing intermolecular interactions the low-temperature deposition also eliminates the influence of mobile substrate atoms present at room temperature.[49-53]

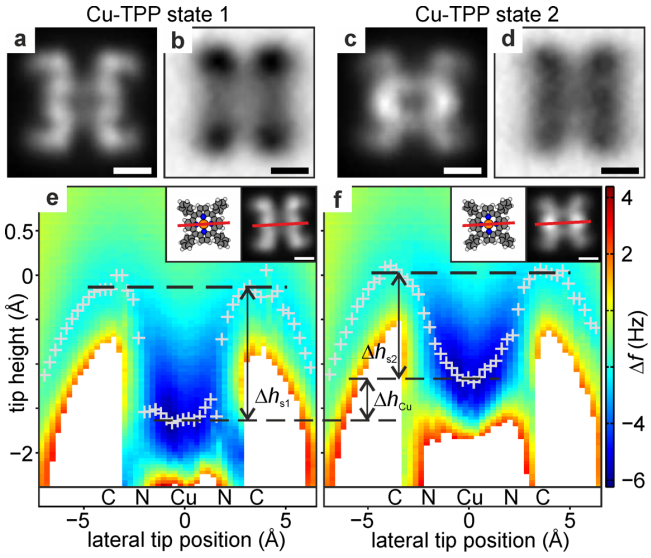

Figure 3. Individual Cu-TPP molecules exhibit conformational bistability. (a,b) After deposition Cu-TPP is exclusively observed in state 1 and (c,d) can then be switched to state 2 by the STM/AFM tip. The differences are most prominent in the current channel during constant-height scans (a,c) but equivalently appear in the simultaneously recorded frequency shift channel (b,d). (e,f) Vertical

images of Cu-TPP state 1 and state 2, respectively. State 2 exhibits less height difference between the rim and the center of the macrocycle and is therefore assumed to be more flat than state 1 (compare bold dashed lines in (e,f)). Additionally, the height of the Cu center is increased for state 2 (thin dashed lines in (e,f)). Zero at the tip height scale corresponds to the SP height. Constant-height images were recorded at a bias voltage of 100 mV and at a *z*-offset of +1.0 Å with respect to the STM SP of 2 pA and 100 mV on copper. The current images depicted in (a,c) are plotted with the very same gray scale contrast. The same holds true for the AFM data depicted in (b,d). Scale bars are 5 Å. Whereas the vertical movement of the Cu center upon switching eludes conventional imaging, vertical images allow for a quantitative analysis of this movement.

Conformational changes can also be induced for 2H-TPP when scanning at elevated bias voltage (2V), however in an irreversible manner. The resulting conformation is identical to that of 2H-TPP deposited onto the sample held at ambient temperature. This is supported by a comparison to literature values of 2H-TPP and 2H-TPyP in room temperature preparations (see SI Fig S3 for a direct comparison).[12,54,55] In STM, these molecules exhibit a central, elongated protrusion that appears higher than the remaining parts (Fig. 4a). In constant-height FM-AFM data approaching the surface, moieties interact repulsively first at the macrocycle where one would expect strongly tilted iminic pyrroles. Four repulsive spots at the center of the molecule indicate the hydrogen atoms of the iminic pyrroles sticking out furthest from the sample surface (see Fig. 4c). The remainder of the molecule merely appears as an attractive background.

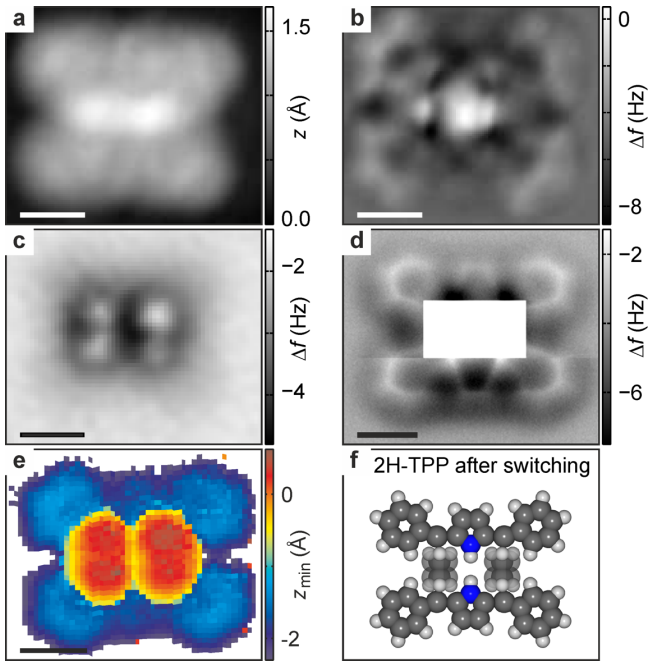

Figure 4. 2H-TPP/Cu(111) after tip-induced conformational changes. (a) Constant-current STM data (SP: I = 23 pA, U = 5 mV). (b) Δf channel recorded simultaneously to the topography depicted in (a): four phenyl rings can be identified in the periphery while the structure in the center cannot be resolved. (c) Constant-height Δf image (SP: I = 2 pA, U = 100 mV on copper): Only four point-like spots at the center of the molecule interact repulsively with the tip in agreement with the four hydrogen atoms of the two iminic pyrrole rings sticking out furthest from the sample. (d) Composed constant-height Δf image from four scans omitting the central area of a molecule deposited onto a sample held at room temperature (0.8 Å retracted with respect to the STM SP: I = 50 pA, U = 5 mV). All molecular moieties shown in this image appear flat and parallel to the sample surface. (e) Map of vertical positions of minima in $\Delta f(z)$ curves. The phenyl rings appear to be (almost) parallel to the sample surface. The z_{min} values at the positions of the upright pyrrole rings appear at ≈ 2 Å larger tip heights as compared to the rest of the molecule. At white pixels the minimum was not reached. A z_{min} value of zero corresponds to an STM SP of 2 pA and 100 mV on copper. Scale bars are 5 Å. (f) Molecular model of 2H-TPP after switching as derived from experimental insights: The molecule is (almost) flat except for the two iminic pyrroles. The exact tilt angle of the upright iminic pyrroles could not be deduced from our experiments, which is therefore depicted with blurriness.

Imaging at closer tip-sample spacing to also resolve the phenyl legs is not possible due to the very upright orientation of the iminic pyrroles. To evade this limitation of constant-height imaging, an activated STM z-feedback can be used to prevent a tip crash while following the surface contour at very close distances (low bias-, high current-setpoint). So far, this method was used to determine adsorption sites of molecules on insulating films.[27,56] In the Δf-channel (Fig. 4b) the phenyls can be clearly distinguished as rings in the periphery, however the structure in the center as described before is lost. Furthermore, Δf signal may be heavily affected by tip-height variations along the constant-current contour. Nevertheless, this technique can supply very fast (preliminary) structure determination of strongly deformed molecules. The structure of the lower lying parts can be confirmed when omitting the molecular center and inspecting only the periphery in constant height. The phenyl legs feature the ring-shaped contrast (Fig. 4d) well-known from related, extensively studied flat-lying hydrocarbon cyclic systems[23,24,28,30]. Interestingly, at the long edges of the molecule a three-segment bridge in between two phenyls can be identified. Such a contrast matches expectations for nearly planar pyrroles of the macrocycle. This allows the suggestion that the macrocycle is strongly deformed with the iminic pyrroles strongly tilted upright and the aminic pyrroles nearly flat while the phenyl legs are rotated almost coplanar to the surface. Furthermore, to avoid the repulsive regime of the nearly flat aminic pyrroles' periphery, the legs rearrange parallel to the surface as evidenced by the rectangular outline of the molecules. This structure model is

supported by mapping the minima of Δ*f*(*z*) curves on a dense grid across the entire molecule[33] – see Fig. 4e. The pertaining map shows two features: In the center, the Δ*f*(*z*) minima appear at a height of ≈ 0.5 Å consistent with the iminic pyrroles sticking out. At the positions of the phenyl legs, the minimum values are ≈ 2 Å closer to the sample and the contrast is very homogenous. The reduced contrast within this area is in line with the phenyl rings being co-planar to the surface. In addition, the contrast at positions of the aminic pyrroles is flat and shows very similar values as for the phenyl legs. We note that a quantitative comparison of minima positions in Δ*f*-curves between phenyl legs and iminic pyrroles is not possible due to the different chemical species at different positions of the molecule interacting with the tip. The findings of very upright iminic pyrroles and planar legs are consistent with NEXAFS data on 2H-TPP / Cu(111)[17], however, the nearly flat orientation of the aminic pyrroles is revealed in this study for the first time. The resulting conformation represents an extreme case for distortions of surface-confined tetrapyrrole species[6,48] though further studies are required to completely disentangle its intricate nature and potential role or appearance in 2D assemblies.

A tip-induced chemical reaction can be ruled out as cause of the changes as STM data of flattened TPP species that underwent cyclodehydrogenation appear distinctly different.[8] It has been shown before that the related tetrapyrrole species can adapt two different conformations upon adsorption onto metal substrates[32,35,54,57], however the structural assignment was based on STM data that convolutes topography and electronic structure and require model calculations for data interpretation. Theoretical support is also essential for space-averaging NEXAFS measurements to disentangle the contributions from different molecular moieties if the individual resonances overlap.[17] In contrast, high-resolution FM-AFM can provide direct access to the adsorption conformation and to the orientation of molecular moieties in real space and is therefore an ideal tool for the investigation of strongly deformed molecules with multiple degrees of freedom. Utilizing tip-induced conformational switching, FM-AFM even allows for the direct structural analysis of conformational transformations at the single-molecule level.

Summarizing, we presented subtle differences in the adsorption geometry of individual 2H-TPP and Cu-TPP molecules when deposited onto a low-temperature substrate. The macrocycle of 2H-TPP appears to be flatter than the one of Cu-TPP, which differs markedly from previous NEXAFS results for monolayer molecular coverages at room temperature. Furthermore tip-induced reversible conformational switching of Cu-TPP reveals bistability along with a vertical movement of the Cu center. The study is complemented by the observation of structural adaptations of 2H-TPP exhibiting an extremely deformed macrocycle along with nearly flat phenyl legs. By comparison to room-

temperature preparations, this conformation could be identified as the energetically favored one. As a novel technique to discriminate and identify conformationally similar species, vertical images, mapping $\Delta f(z)$ minima in planes perpendicular to the sample surface, were introduced. The applied experimental techniques refine the understanding of the molecular systems and provide information neither accessible by STM imaging nor space-averaging experiments. FM-AFM can therefore be employed as a powerful tool for the structural analysis of strongly deformed molecules with a pronounced 3D-character and their identification – in many cases without requiring sophisticated simulations for data analysis. By using tip functionalization less flexible than a CO molecule, quantitative (out of surface plane) tilt angle determinations – even along non high symmetry directions or along molecular moieties – may be possible in the future. Thus, our study opens novel pathways to quantitatively determine the conformation of complex and flexible surface-anchored species on the single-molecule level using lab-based FM-AFM, giving access to subtle structural differences and conformational transformations.

Experimental Procedures

Experiments were performed using a home-built combined STM/AFM operated in ultra-high vacuum ($p \approx 5 \times 10^{-11}$ mbar) at low temperature of ≈ 5K. The microscope is equipped with a qPlus sensor[58] and operated in the frequency modulation mode[59]. The oscillation amplitude was fixed to 0.5 Å to increase the lateral resolution[60] and bias voltages refer to the sample with respect to the tip. Individual 2H-TPP and Cu-TPP molecules (Sigma-Aldrich) were sublimed onto the cold Cu(111) surface with the sample being located inside the scanner. All data was recorded using a CO functionalized tip[23]. To facilitate the CO pickup, a small amount of bilayer NaCl islands were grown. A CO transfer from the NaCl islands to the tip can be achieved by approaching the tip at a CO several hundred pm from a typical setpoint of I = 10 pA, U = 100 mV. All data was recorded away from the NaCl islands on copper. The $\Delta f(z)$-grid on the switched 2H-TPP molecules contains 50 times 50 pixels and was recorded with disabled z-feedback. To correct for lateral drift and creep during the 15 hours of data acquisition, we recorded a constant-height image after each line of spectra. In the data analysis, a cross correlation procedure of these images allowed to correct for lateral mismatch by shifting the grid pixels accordingly. In order to record all $\Delta f(z)$ spectra for the grid as well as the vertical images in a sufficiently close but safe distance regime, we implemented a threshold criterion as introduced by Mohn et al.[41] Additional data was recorded on 2H-TPP molecules, which were sublimed from a quartz crucible onto a sample held at room temperature. These experiments were carried out in a separate apparatus (CREATEC LT-STM/AFM) under comparable experimental

conditions ($p \approx 2 \times 10^{-10}$ mbar, T ≈ 5K, qPlus with oscillation amplitude fixed to 0.8 Å, CO functionalized tip).

Acknowledgment

We thank Andreas Pöllmann for help. We acknowledge financial support from the Deutsche Forschungsgemeinschaft (SPP 1243, RE 2669/4-1), the Volkswagenstiftung through its 'Lichtenberg Programm' and the European Research Council (ERC) Advanced Grant MolArt (no. 247299). W.A. acknowledges funding by the DFG via a Heisenberg professorship and by the ERC Consolidator Grant NanoSurfs (no. 615233).

Supporting Information

Additional vertical images along the second mirror plane of 2H-TPP and Cu-TPP in both states as well as a direct comparison of 2H-TPP deposited on the sample surface held at room temperature and the switched species after low temperature deposition are provided. This material is available free of charge via the Internet at http://pubs.acs.org.

Conflict of interest

The authors declare no competing financial interest.

(1) Sedona, F.; Di Marino, M.; Forrer, D.; Vittadini, A.; Casarin, M.; Cossaro, A.; Floreano, L.; Verdini, A.; Sambi, M. *Nature Materials* **2012**, *11*, 970.

(2) Auwärter, W.; Seufert, K.; Bischoff, F.; Ecija, D.; Vijayaraghavan, S.; Joshi, S.; Klappenberger, F.; Samudrala, N.; Barth, J. V. *Nature Nanotechnology* **2012**, *7*, 41.

(3) Wäckerlin, C.; Tarafder, K.; Girovsky, J.; Nowakowski, J.; Hählen, T.; Shchyrba, A.; Siewert, D.; Kleibert, A.; Nolting, F.; Oppeneer, P. M.; Jung, T. A.; Ballav, N. *Angewandte Chemie International Edition* **2013**, *52*, 4568.

(4) Gottfried, J. M. *Surface Science Reports* **2015**, *70*, 259.

(5) Gottfried, M.; Marbach, H. *Z. Phys. Chem.* **2009**, *223*, 53.

(6) Auwärter, W.; Écija, D.; Klappenberger, F.; Barth, J. V. *Nature Chemistry* **2015**, *7*, 105.

(7) Buchner, F.; Zillner, E.; Röckert, M.; Gläßel, S.; Steinrück, H.-P.; Marbach, H. *Chemistry – A European Journal* **2011**, *17*, 10226.

(8) Wiengarten, A.; Lloyd, J. A.; Seufert, K.; Reichert, J.; Auwärter, W.; Han, R.; Duncan, D. A.; Allegretti, F.; Fischer, S.; Oh, S. C.; Sağlam, Ö.; Jiang, L.; Vijayaraghavan, S.; Écija, D.; Papageorgiou, A. C.; Barth, J. V. *Chemistry – A European Journal* **2015**, *21*, 12285.

(9) Joshi, S.; Bischoff, F.; Koitz, R.; Ecija, D.; Seufert, K.; Seitsonen, A. P.; Hutter, J.; Diller, K.; Urgel, J. I.; Sachdev, H.; Barth, J. V.; Auwärter, W. *ACS Nano* **2014**, *8*, 430.

(10) Bischoff, F.; Seufert, K.; Auwärter, W.; Joshi, S.; Vijayaraghavan, S.; Écija, D.; Diller, K.; Papageorgiou, A. C.; Fischer, S.; Allegretti, F.; Duncan, D. A.; Klappenberger, F.; Blobner, F.; Han, R.; Barth, J. V. *ACS Nano* **2013**, *7*, 3139.

(11) Auwärter, W.; Seufert, K.; Klappenberger, F.; Reichert, J.; Weber-Bargioni, A.; Verdini, A.; Cvetko, D.; Dell'Angela, M.; Floreano, L.; Cossaro, A.; Bavdek, G.; Morgante, A.; Seitsonen, A. P.; Barth, J. V. *Physical Review B* **2010**, *81*, 245403.

(12) Auwärter, W.; Klappenberger, F.; Weber-Bargioni, A.; Schiffrin, A.; Strunskus, T.; Wöll, C.; Pennec, Y.; Riemann, A.; Barth, J. V. *Journal of the American Chemical Society* **2007**, *129*, 11279.

(13) Weber-Bargioni, A.; Auwärter, W.; Klappenberger, F.; Reichert, J.; Lefrançois, S.; Strunskus, T.; Wöll, C.; Schiffrin, A.; Pennec, Y.; Barth, J. V. *ChemPhysChem* **2008**, *9*, 89.

(14) Xiao, J.; Ditze, S.; Chen, M.; Buchner, F.; Stark, M.; Drost, M.; Steinrück, H.-P.; Gottfried, J. M.; Marbach, H. *The Journal of Physical Chemistry C* **2012**, *116*, 12275.

(15) Stark, M.; Ditze, S.; Drost, M.; Buchner, F.; Steinrück, H.-P.; Marbach, H. *Langmuir* **2013**, *29*, 4104.

(16) Röckert, M.; Ditze, S.; Stark, M.; Xiao, J.; Steinrück, H.-P.; Marbach, H.; Lytken, O. *The Journal of Physical Chemistry C* **2014**, *118*, 1661.

(17) Diller, K.; Klappenberger, F.; Marschall, M.; Hermann, K.; Nefedov, A.; Wöll, C.; Barth, J. V. *The Journal of Chemical Physics* **2012**, *136*, 014705.

(18) Seufert, K.; Bocquet, M.-L.; Auwärter, W.; Weber-Bargioni, A.; Reichert, J.; Lorente, N.; Barth, J. V. *Nature Chemistry* **2011**, *3*, 114.

(19) Klappenberger, F. *Progress in Surface Science* **2014**, *89*, 1.

(20) Houwaart, T.; Le Bahers, T.; Sautet, P.; Auwärter, W.; Seufert, K.; Barth, J. V.; Bocquet, M.-L. *Surface Science* **2015**, *635*, 108.

(21) Auwärter, W.; Weber-Bargioni, A.; Riemann, A.; Schiffrin, A.; Gröning, O.; Fasel, R.; Barth, J. V. *The Journal of Chemical Physics* **2006**, *124*, 194708.

(22) Gross, L.; Mohn, F.; Moll, N.; Schuler, B.; Criado, A.; Guitián, E.; Peña, D.; Gourdon, A.; Meyer, G. *Science* **2012**, *337*, 1326.

(23) Gross, L.; Mohn, F.; Moll, N.; Liljeroth, P.; Meyer, G. *Science* **2009**, *325*, 1110.

(24) Albrecht, F.; Pavliček, N.; Herranz-Lancho, C.; Ruben, M.; Repp, J. *Journal of the American Chemical Society* **2015**, *137*, 7424.

(25) Albrecht, F.; Neu, M.; Quest, C.; Swart, I.; Repp, J. *Journal of the American Chemical Society* **2013**, *135*, 9200.

(26) Hanssen, K. Ø.; Schuler, B.; Williams, A. J.; Demissie, T. B.; Hansen, E.; Andersen, J. H.; Svenson, J.; Blinov, K.; Repisky, M.; Mohn, F.; Meyer, G.; Svendsen, J.-S.; Ruud, K.; Elyashberg, M.; Gross, L.; Jaspars, M.; Isaksson, J. *Angewandte Chemie International Edition* **2012**, *51*, 12238.

(27) Pavliček, N.; Fleury, B.; Neu, M.; Niedenführ, J.; Herranz-Lancho, C.; Ruben, M.; Repp, J. *Physical Review Letters* **2012**, *108*, 086101.

(28) Riss, A.; Wickenburg, S.; Gorman, P.; Tan, L. Z.; Tsai, H.-Z.; de Oteyza, D. G.; Chen, Y.-C.; Bradley, A. J.; Ugeda, M. M.; Etkin, G.; Louie, S. G.; Fischer, F. R.; Crommie, M. F. *Nano Letters* **2014**, *14*, 2251.

(29) van der Lit, J.; Boneschanscher, M. P.; Vanmaekelbergh, D.; Ijäs, M.; Uppstu, A.; Ervasti, M.; Harju, A.; Liljeroth, P.; Swart, I. *Nature Communications* **2013**, *4*.

(30) Oteyza, D. G. d.; Gorman, P.; Chen, Y.-C.; Wickenburg, S.; Riss, A.; Mowbray, D. J.; Etkin, G.; Pedramrazi, Z.; Tsai, H.-Z.; Rubio, A.; Crommie, M. F.; Fischer, F. R. *Science* **2013**, *340*, 1434.

(31) Schuler, B.; Fatayer, S.; Mohn, F.; Moll, N.; Pavliček, N.; Meyer, G.; Peña, D.; Gross, L. *Nature Chemistry* **2016**, *8*, 220.

(32) Jarvis, S. P.; Taylor, S.; Baran, J. D.; Champness, N. R.; Larsson, J. A.; Moriarty, P. *Nature Communications* **2015**, *6*, 8338.

(33) Schuler, B.; Liu, W.; Tkatchenko, A.; Moll, N.; Meyer, G.; Mistry, A.; Fox, D.; Gross, L. *Physical Review Letters* **2013**, *111*, 106103.

(34) Moreno, C.; Stetsovych, O.; Shimizu, T. K.; Custance, O. *Nano Lett.* **2015**, *15*, 2257.

(35) Jarvis, S. P.; Taylor, S.; Baran, J. D.; Thompson, D.; Saywell, A.; Mangham, B.; Champness, N. R.; Larsson, J. A.; Moriarty, P. *The Journal of Physical Chemistry C* **2015**, *119*, 27982.

(36) Kawai, S.; Sadeghi, A.; Okamoto, T.; Mitsui, C.; Pawlak, R.; Meier, T.; Takeya, J.; Goedecker, S.; Meyer, E. *Small* **2016**, *12*, 5303.

(37) Wölfle, T.; Görling, A.; Hieringer, W. *Physical Chemistry Chemical Physics* **2008**, *10*, 5739.

(38) Diller, K.; Papageorgiou, A. C.; Klappenberger, F.; Allegretti, F.; Barth, J. V.; Auwärter, W. *Chemical Society Reviews* **2016**, *45*, 1629.

(39) Pavliček, N.; Herranz-Lancho, C.; Fleury, B.; Neu, M.; Niedenführ, J.; Ruben, M.; Repp, J. *physica status solidi (b)* **2013**, *250*, 2424.

(40) Moll, N.; Gross, L.; Mohn, F.; Curioni, A.; Meyer, G. *New Journal of Physics* **2010**, *12*, 125020.

(41) Mohn, F.; Gross, L.; Meyer, G. *Applied Physics Letters* **2011**, *99*, 053106.

(42) van der Heijden, N. J.; Hapala, P.; Rombouts, J. A.; van der Lit, J.; Smith, D.; Mutombo, P.; Švec, M.; Jelinek, P.; Swart, I. *ACS Nano* **2016**, *10*, 8517.

(43) Qiu, X. H.; Nazin, G. V.; Ho, W. *Physical Review Letters* **2004**, *93*, 196806.

(44) Moresco, F.; Meyer, G.; Rieder, K.-H.; Tang, H.; Gourdon, A.; Joachim, C. *Physical Review Letters* **2001**, *86*, 672.

(45) Auwärter, W.; Seufert, K.; Klappenberger, F.; Reichert, J.; Weber-Bargioni, A.; Verdini, A.; Cvetko, D.; Dell' Angela, M.; Floreano, L.; Cossaro, A.; others *Phys. Rev. B* **2010**, *81*, 245403.

(46) Buchner, F.; Kellner, I.; Hieringer, W.; Görling, A.; Steinrück, H.-P.; Marbach, H. *Physical Chemistry Chemical Physics* **2010**, *12*, 13082.

(47) Brede, J.; Linares, M.; Kuck, S.; Schwöbel, J.; Scarfato, A.; Chang, S.-H.; Wiesendanger, R.; Lensen, R.; Kouwer, P. H. J.; Hoogboom, J.; Rowan, A. E.; Funk, M.; Stafström, S.; Zerbetto, F.; Lazzaroni, R. *Nanotechnology* **2009**, *20*, 275602.

(48) Donovan, P.; Robin, A.; Dyer, M. S.; Persson, M.; Raval, R. *Chemistry – A European Journal* **2010**, *16*, 11641.

(49) Stoltze, P. *Journal of Physics: Condensed Matter* **1994**, *6*, 9495.

(50) Repp, J.; Moresco, F.; Meyer, G.; Rieder, K.-H.; Hyldgaard, P.; Persson, M. *Physical Review Letters* **2000**, *85*, 2981.

(51) Mielke, J.; Hanke, F.; Peters, M. V.; Hecht, S.; Persson, M.; Grill, L. *J. Am. Chem. Soc.* **2015**, *137*, 1844.

(52) Klappenberger, F.; Weber-Bargioni, A.; Auwärter, W.; Marschall, M.; Schiffrin, A.; Barth, J. V. *The Journal of Chemical Physics* **2008**, *129*, 214702.

(53) Eichberger, M.; Marschall, M.; Reichert, J.; Weber-Bargioni, A.; Auwarter, W.; Wang, R. L. C.; Kreuzer, H. J.; Pennec, Y.; Schiffrin, A.; Barth, J. V. *Nano letters* **2008**, *8*, 4608.

(54) Rojas, G.; Simpson, S.; Chen, X.; Kunkel, D. A.; Nitz, J.; Xiao, J.; Dowben, P. A.; Zurek, E.; Enders, A. *Physical Chemistry Chemical Physics* **2012**, *14*, 4971.

(55) Ditze, S.; Stark, M.; Drost, M.; Buchner, F.; Steinrück, H.-P.; Marbach, H. *Angewandte Chemie International Edition* **2012**, *51*, 10898.

(56) Gross, L.; Mohn, F.; Moll, N.; Meyer, G.; Ebel, R.; Abdel-Mageed, W. M.; Jaspars, M. *Nature Chemistry* **2010**, *2*, 821.

(57) Iancu, V.; Deshpande, A.; Hla, S.-W. *Nano Lett.* **2006**, *6*, 820.

(58) Giessibl, F. J. *Applied Physics Letters* **2000**, *76*, 1470.

(59) Albrecht, T. R.; Grütter, P.; Horne, D.; Rugar, D. *Journal of Applied Physics* **1991**, *69*, 668.

(60) Giessibl, F. J. *Reviews of Modern Physics* **2003**, *75*, 949.

TOC figure:

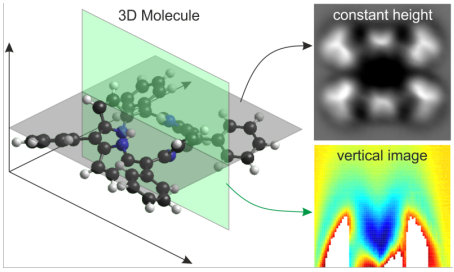
3D Molecule
constant height
vertical image